THE ASTROPHYSICAL JOURNAL, 396:273–288, 1992 September 1

EXPLORING THE PECULIAR MAGNETIC FIELD OF FEIGE 7

N. ACHILLEOS[1]
Mount Stromlo and Siding Spring Observatories, Australian National University

D. T. WICKRAMASINGHE
Department of Mathematics, Australian National University, G.P.O. Box 4, Canberra, ACT Australia 2601

JAMES LIEBERT AND REX A. SAFFER
Steward Observatory, University of Arizona, Tucson, AZ 85721

AND

A. D. GRAUER
Department of Physics and Astronomy, University of Arkansas, 2801 South University Avenue, Little Rock, AR 72204
Received 1991 November 20; accepted 1992 March 9

ABSTRACT

We present time-resolved, high signal-to-noise intensity spectra for the magnetic white dwarf Feige 7. On the basis of these data, we show, using computer models for magnetic stars, that the magnetic field in Feige 7 cannot be represented by a centered dipole geometry. We find that a good approximation to the field is a dipole of strength 35 MG displaced by 0.15 white dwarf radii from the stellar center, viewed at different angles as the star rotates. Furthermore, we find it necessary to use a model with variable surface abundances of hydrogen and helium to reproduce the variation, due to stellar rotation, in the Zeeman absorption lines of these elements.

Subject headings: stars: individual (Feige 7) — stars: magnetic fields — stars: white dwarfs

1. INTRODUCTION

Feige 7 (L795 – 7, Gr 267, WD 0041 – 102) is an isolated magnetic white dwarf. It is the only member of this class of stars, comprising ~25 objects (for recent reviews see Schmidt 1987 and Wickramasinghe 1987), which shows significant Zeeman absorption lines of helium as well as hydrogen. Furthermore, both the spectrum and the circular polarization of Feige 7 vary periodically, as shown by Liebert et al. (1977, hereafter L77). This variability is interpreted as the result of stellar rotation. Rotation presents different sections of the magnetic geometry of Feige 7 with time, leading to the observed variations in intensity and polarization.

L77 used their data to deduce the range of magnetic field strengths present in the atmosphere of Feige 7. They used the tables by Kemic (1974), which give wavelength positions of hydrogen and helium absorption lines as a function of magnetic field strength. Subsequently, Martin & Wickramasinghe (1986, hereafter MW) performed a more detailed analysis using models for magnetic white dwarfs similar to those used in this paper. They confirmed the following original conclusions of L77:

1. *Composition and Temperature.*—Helium is the dominant atmospheric element present in Feige 7. The effective temperature for the star is approximately 20,000 *K*. The best estimate of an effective temperature is 21,000 ± 2000 *K* from Greenstein & Oke (1982). This estimate is based on fitting the *IUE* and optical energy distribution with the pure hydrogen and mixed helium and hydrogen atmospheric models from Wickramasinghe (1972). There is a consistent estimate, based on optical spectra, in Greenstein & Boksenberg (1978).

2. *Zeeman Lines of* H *and* He.—Line identifications for the H and He Zeeman components in Feige 7 were included in the studies by L77 and MW. Both sets of identifications agreed in the majority of cases as to which particular transition gave rise to the line in question. However, L77 proposed a region with field strengths in the range 18–20 MG for the formation of particular components. The models of MW showed that the same components could be reproduced using a dipole field, with strengths varying between 17.5 MG (at the magnetic equator) to 35 MG (at the magnetic poles).

3. *Viewing Geometry.*—The studies by L77 and by MW independently established a viewing geometry for Feige 7. These were described in terms of the range of angles between the observer's line of sight and the star's magnetic axis of symmetry. Both studies yielded a range of viewing angles between ~60° and ~120°.

The major shortcoming in the modeling of Feige 7 done by MW was related to the large shifts, observed by L77, of some Zeeman lines in the blue spectral region ($\lambda\lambda$4300–5300). The shifts during one period were up to 15 Å in some cases. MW found that, if they were to keep reasonable agreement with the circular polarization data, they could *not* reproduce these line shifts using a rotating centered dipole field *nor* a rotating offset dipole field.

It is the purpose of this paper to present recent time-resolved, high-quality spectra of Feige 7 and to use these as a basis for an independent modeling study of this star. We find that a rotating offset dipole field *is* consistent with these observations. In § 2, we briefly describe the key elements of the models which we synthesized for our analysis. Section 3 presents the observational data for Feige 7 which form the basis for our interpretations. Sections 4 and 5 compare theory and observation in detail, and § 6 contains a discussion and outline of important results.

[1] Postal address: Département de Physique, Université de Montréal, C.P. 6128, Succ. A, Montréal, Quebec, Canada H3C 3J7.

2. MODEL DESCRIPTION

The physical ingredients of the magnetic white dwarf models used in this paper have been described most recently in the study by Achilleos & Wickramasinghe (1989). We briefly reiterate some of the important features of our models here, with particular emphasis on their application to the special case of Feige 7.

2.1. *Field Geometry*

Our models all assume a dipolar magnetic field structure. The distribution of magnetic field strengths and directions over the surface of our model stars is generated by dipoles situated at the stellar center or displaced from the stellar center. Consider the coordinate system shown in Figure 1. The z-axis is parallel to the magnetic axis of symmetry, or dipole axis. The x-axis is orthogonal to the z direction and lies in the same plane as the z-axis and the observer's line of sight. The y-axis is orthogonal to these other axes and completes the system. The center of the model white dwarf is located at the origin. The magnetic dipole itself is displaced a distance of a_z radii away from the center, along the z-axis. We only consider z offsets in this paper. Achilleos & Wickramasinghe (1989) have discussed offsets along the x- and y-axes. If we adopt the white dwarf radius, R_{wd}, as our unit of distance, the following expression gives the Cartesian field components at the point with coordinates (x, y, z):

$$B_x = 3B_d\, x(z - a_z)/2r^5 \quad (1)$$

$$B_y = 3B_d\, y(z - a_z)/2r^5 \quad (2)$$

$$B_z = B_d[3(z - a_z)^2 - r^2]/2r^5 , \quad (3)$$

where $r = [x^2 + y^2 + (z - a_z)^2]^{1/2}$ is the distance from the location of the dipole (magnetic center of the star). The quantity B_d is the dipole strength which, for the case of a centered dipole ($a_z = 0$), is equal to the field strength at the magnetic poles of the star [where $(x, y, z) = (0, 0, \pm 1)$]. The expression for the total field strength B at point (x, y, z) is

$$B = B_d[1 + 3(z - a_z)^2/r^2]^{1/2}/2r^3 . \quad (4)$$

If we introduce the coordinates θ and R defined by the relations

$$z = R\cos\theta$$

$$R^2 = x^2 + y^2 + z^2$$

$$r^2 = R^2 - 2a_z R\cos\theta + a_z^2 . \quad (5)$$

Then we may rewrite the expression for the total field strength as follows:

$$B = B_d/2r^4[R^2(1 + 3\cos^2\theta) + 4a_z(a_z - 2R\cos\theta)]^{1/2} , \quad (6)$$

where R is the distance from the white dwarf center and θ is the angle between the z-axis and the position vector of the point in question. We refer to θ as the magnetic latitude.

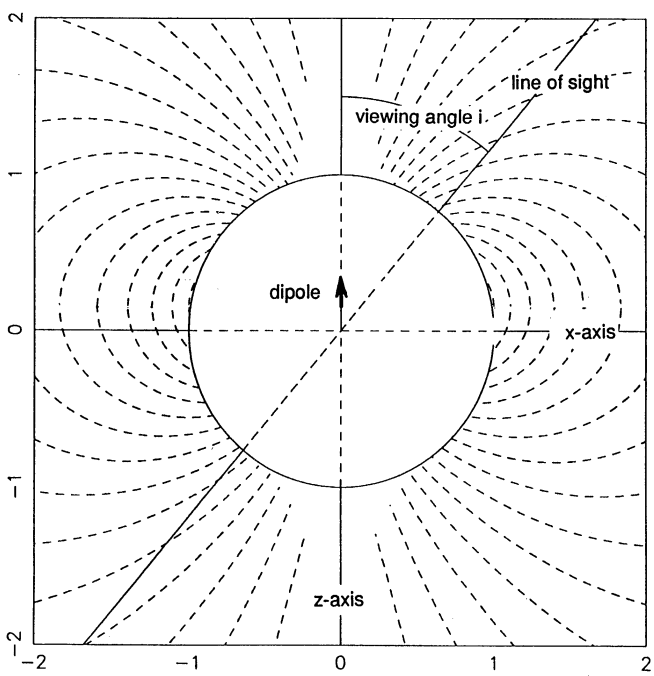

FIG. 1.—Coordinates for field calculations. The coordinate system used to calculate the field distributions of magnetic white dwarf models. Field lines shown are generated by a dipole displaced 0.15 white dwarf radii along the z-axis.

Figure 2 shows the field strength B at the surface ($R = 1$), plotted as a function of magnetic latitude, for a centered dipole field and an offset dipole with the displacement $a_z = 0.1$. For the case of the centered dipole, we see that B decreases by a factor of 2 as we go from poles ($\theta = 0°$, 180°) to equator ($\theta = 90°$). The slope of the curve shows that the equator and poles are also the regions where the field strength varies least rapidly with magnetic latitude.

If we now look at the offset dipole, we see that the range of surface field strengths has increased above a factor of 2 to a factor of almost 3 between equator and north ($\theta = 0°$) pole. On the other hand, the field strength at the south ($\theta = 180°$) pole has decreased to about three quarters of its original value. We also notice that the field spread at latitudes around 45° increases as the dipole is displaced closer to the north pole (we take this to be a positive value for a_z). At the same time, the region around $\theta = 135°$ is now further from the dipole and develops a more uniform field distribution.

The lower part of the graph in Figure 2 shows the surface area at each latitude projected in the direction of an observer whose line of sight makes angles of $i = 0°$ and 90° with the dipole axis. These angles represent the "pole-on" and "equator-on" views of the star, respectively. We see, as we expect, that the case $i = 90°$ gives most weight to the equatorial latitudes and fields. This means that the observer sees a relatively uniform field distribution. However, the view for which $i = 0°$ and the observer looks at the pole gives most weight to those latitudes where the field spread is largest. The "pole-on" view also favors field strengths larger than those associated with the "equator-on" view.

We conclude this section by noting that the two parameters which influence the effective spread in fields presented to an observer are, first, the amount of offset associated with the dipole, and, second, the observer's viewing angle i.

2.2. *Atmospheric Composition and Structure*

The models we synthesized for the purpose of analyzing the data for Feige 7 involved solving the problem of the transfer of polarized radiation through a magnetized atmosphere. We assume that the temperature and pressure structure of this atmosphere is *not affected* by the presence of the magnetic field. Jordan (1988) has argued that the field has negligible influence

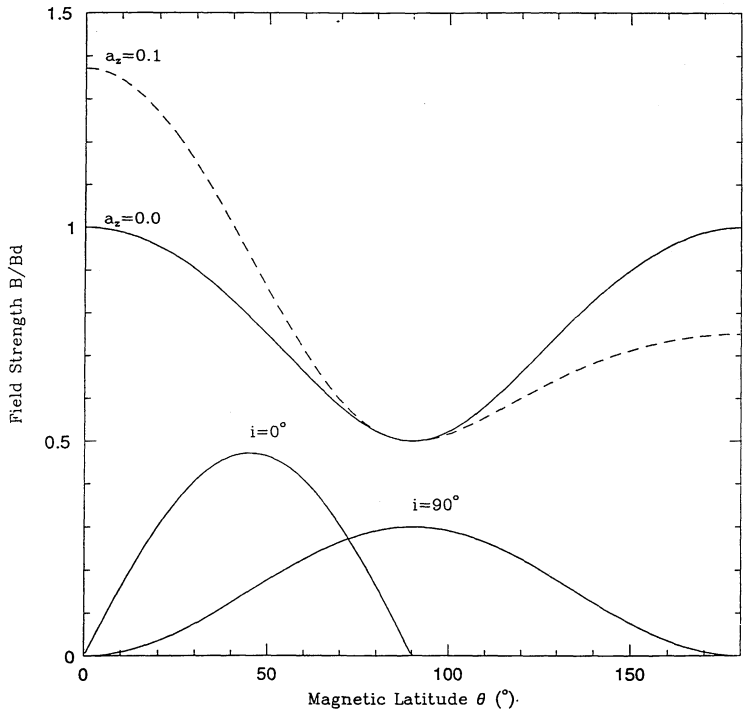

FIG. 2.—Behavior of dipole fields. The upper plots show surface field strength B (in units of dipole strength B_d) versus magnetic latitude θ for centered and offset dipole fields. The lower plots show a relative measure of the visible surface area at each latitude projected in the direction of an observer whose line of sight makes angles of $i = 0°$ and $i = 90°$ to the z-axis.

on atmospheric structure for fields less than ~100 MG. He reached this conclusion using the theoretical arguments by Landstreet (1987) which described the magnitude of the currents induced in the outer layers of magnetic stars as a result of the decay of the global magnetic field.

The largest field strength associated with Feige 7's atmosphere is about 57 MG (from the results of this paper). This distinguishes it as a star whose magnetic field, according to Jordan's picture, has negligible effect on its atmospheric structure and for which a zero-field atmosphere is a safe assumption for the purpose of modeling.

The zero-field atmospheres used for this study were all calculated using a surface gravity of $g = 10^8$ cm s^{-2}, commonly used for white dwarfs. The compositions of our model atmospheres were a mixture of hydrogen and helium. They were all calculated using the ATLAS program by Kurucz (1971). Those including helium used the structure by Wickramasinghe (1972) as a "starting model," which was then subject to the iterative calculations required to produce a "converged" atmospheric model.

2.3. *Radiative Transfer*

At each point on the visible surface of our model white dwarf we solved the equations of polarized radiative transfer (Martin & Wickramasinghe 1979) using our zero-field atmospheric structure. This approach yielded solutions for the four Stokes parameters I, Q, U, and V. These parameters specify the intensity and polarization of the radiation. We then summed the contributions for all points on the visible disk, weighting each term by the area of the surface element at each point projected along the observer's line of sight.

We shifted the line and continuum opacities at each point according to the field strength there, using the tables by Kemic (1974) and the method outlined by Lamb & Sutherland (1974). We also included magneto-optical effects in the lines and continuum as described in Martin & Wickramasinghe (1981, 1982). These are terms which describe the change in polarization state due to the phenomenon of birefringence. This refers to the fact that radiation of different polarization states experiences different refractive indices as it propagates.

3. OBSERVATIONS

3.1. *Data Acquisition and Reduction*

Feige 7 was observed on the night of 1990 September 12 with the Multiple Mirror Telescope (MMT) and "Red Channel" spectrograph equipped with an 800 × 800 pixel Texas Instruments CCD detector (Schmidt, Weymann, & Foltz 1989). The configuration used was the low-resolution echellette mode described in that paper, which permits up to seven orders of the spectrum to be measured at 5.6 Å resolution, each covering nearly 1400 Å with some overlap and spanning, in principle, a wavelength interval 4000–9000 Å. Due to the limits imposed by the availability of modern tabulated Zeeman transitions, however, only four orders were combined to produce the final spectra, resulting in total wavelength coverage $\lambda\lambda$4050–6560.

The two-dimensional images were reduced using standard packages in the Image Reduction and Analysis Facility (IRAF). After bias subtraction and trimming, each image was divided by an averaged, normalized image of several flat-field images obtained by observing a diffusing screen illuminated by incandescent lamps. Each aperture in the average flat-field image was normalized by a one-dimensional normalization function derived by extraction of a spectrum from each aperture and fitting with a sixth-order spline. Each pixel along the

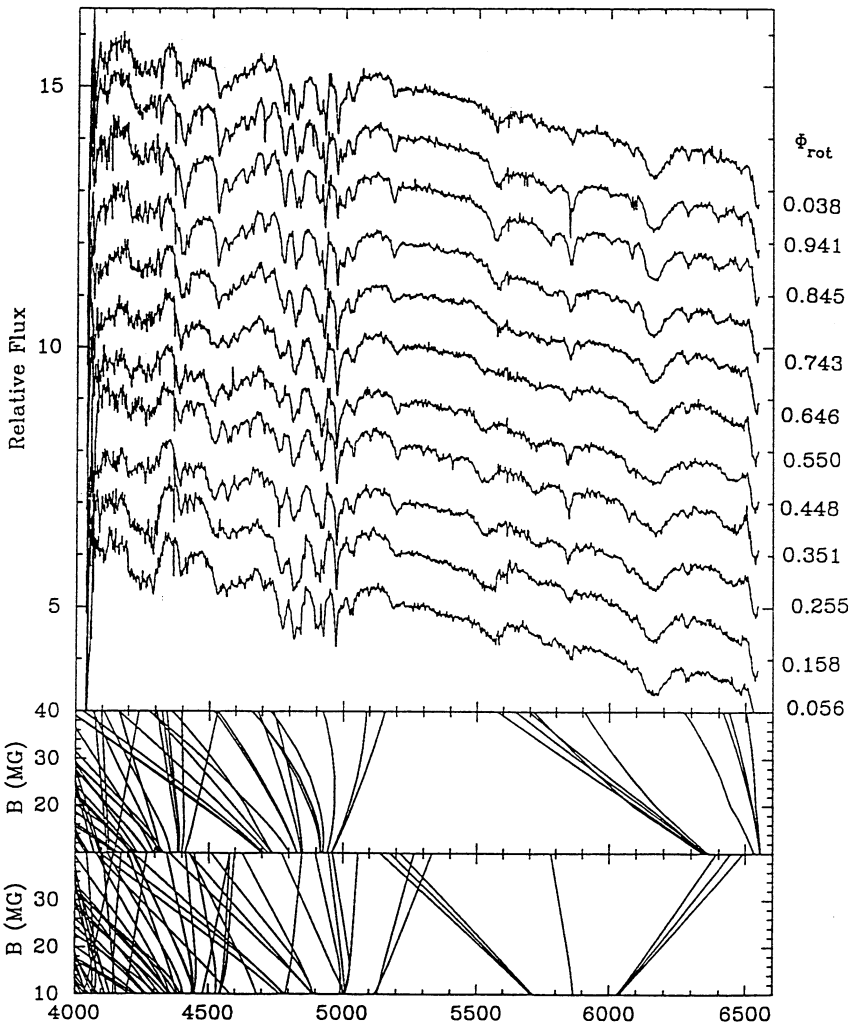

FIG. 3.—Spectra of Feige 7. The time-resolved intensity spectra of Feige 7 observed in 1990 September. The observations have been scaled to the same flux at 5300 Å with the flux zero points shifted for clarity. Each spectrum is labeled with its appropriate rotational phase using the ephemeris of Liebert et al. (1977). Below the observations we have plotted the variation with field strength of the wavelength position of our calculated Zeeman components of H and He.

dispersion direction in each aperture then was divided by the appropriate fitted function. All points outside the apertures were set to unity.

Each spectral order was extracted as a simple sum across the aperture, wavelength calibrated using exposures of a HeAr comparison lamp, and flux calibrated using observations of the standards BD +28 4211 and L1363−3 (Massey et al. 1988; Oke 1974). The flux-calibrated orders then were combined to produce the final spectra. The spectral coverage of the four orders used was (1) 4050–4327 Å, (2) 4327–4902 Å, (3) 4902–5611 Å, and (4) 5611–6560 Å. The splice point between orders was chosen to be the pixel where the number of counts were approximately equal; that is, data in the overlap region from the order having the lesser response was discarded. Discontinuities or sharp features near the splice wavelengths of 4327, 4902, and 5611 Å should not be considered real.

We present in Figure 3 the eleven intensity spectra of Feige 7. The exposure time for each spectrum was 720 s. The rotational period for Feige 7 has been determined from polarimetric observations as being 131.606 minutes (L77). The spectra therefore span a full rotational cycle. Also shown are the rotational phases associated with each spectrum, calculated using the polarization ephemeris of L77. Each phase corresponds to a point in time midway through the exposure.

Feige 7 has also exhibited photometric variations. High-speed photometric observations of Feige 7 covering more than one rotational period were obtained on 1989 September 30 with the *B* filter and on 1989 October 6 with the *V* filter. These observations were made at the University of Arizona 1.55 m reflector at the Catalina Station on Mount Lemmon using the University of Arkansas two star photometer with an EMI 9840B photomultiplier tube for program star and an EMI 9826 tube for the comparison star. Each time series run used 10 s integrations, although no variations appear on anything other than the rotational time scale. The use of a comparison star allows moderate nonphotometric sky conditions and variations due to atmospheric extinction to be divided out.

Figure 4 shows the change in *V*-magnitude of Feige 7 during two rotational cycles. The photometric and polarimetric periods are equal. There is a peak-to-peak variation of about 0.1 mag during each cycle. The variation in *V* takes the form of a small "pulse" (about 0.05 mag high) followed by a larger one (about 0.1 mag high). Each pulse persists for roughly half a period. Any satisfactory model for Feige 7 must reproduce

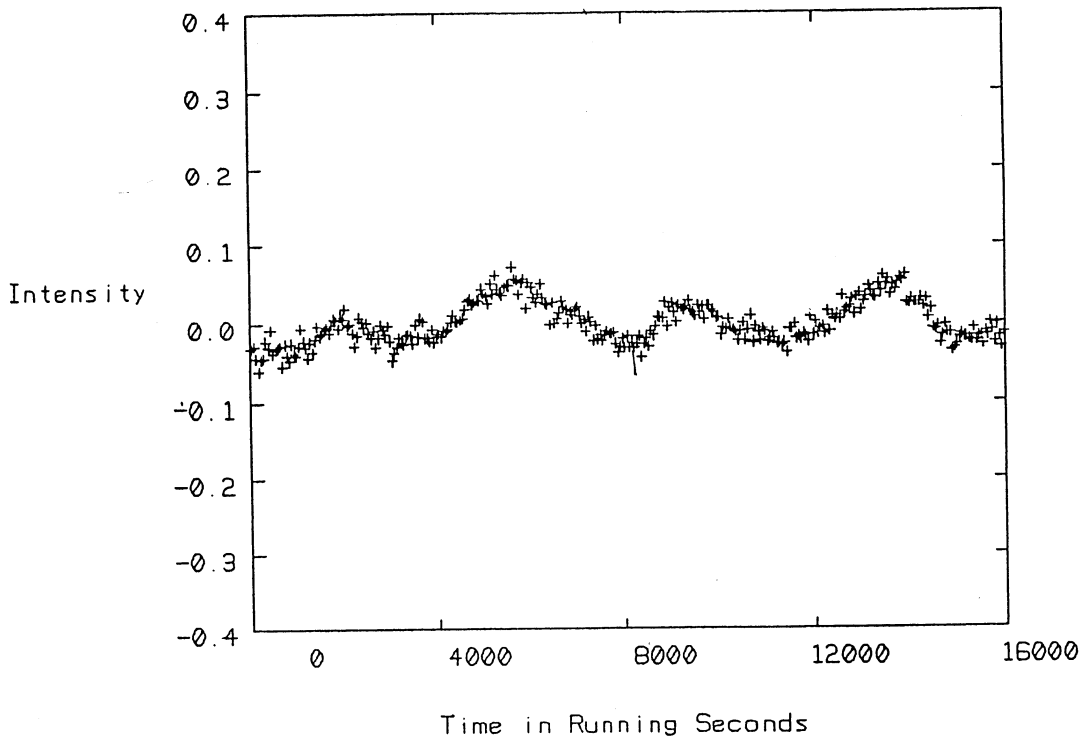

FIG. 4.—Photometry of Feige 7. The variation in V-magnitude of Feige 7 about the mean value, which is shown as the zero point. Higher points on the plot correspond to brighter light levels.

such photometric variability in addition to the observed variations in polarization and spectral features.

3.2. *Line Identifications*

Figure 3 shows a spectrum rich in absorption line structure. As we have mentioned, these absorption complexes are single or blended Zeeman components of hydrogen and helium. A knowledge of how each of these components shifts in wavelength with magnetic field strength enables us to extract useful information about the surface field distribution of Feige 7.

To illustrate this point, we have plotted below the spectra in Figure 3 our interpolations from the tables of Kemic (1974) for the wavelength positions of Zeeman H and He lines as a function of field strength. If we consider a centered dipole field with a strength of 35 MG at the poles, the total range of field strengths over which the Zeeman lines are formed will be from 17.5 MG at the magnetic equator to 35 MG at the poles. Figure 3 shows us that this range of field strengths is compatible with the positions of H and He Zeeman lines in the observed spectra.

In Figure 5, we show the observed spectrum at phase $\Phi_{rot} = 0.038$ plotted above the synthetic spectrum of a centered dipole field with $B_d = 35$ MG viewed at $i = 90°$. The model star threaded by this field has an atmosphere containing helium and hydrogen in the ratio He:H = 100 (ratio of number densities). Below the synthetic spectrum, we have indicated the particular transitions which are major contributors (have largest line strengths) to the observed absorption lines.

The model reproduces the appearance of the forest of lines blueward of 5000 Å due to Hβ, Hγ, and He λ4471 line components. The relative strengths of these blue Zeeman features match those observed, except for the Hβ line at $\sim$4980 Å, whose synthetic profile is too strong to match the data.

The part of the spectrum redward of 5000 Å contains absorption lines due to He λ5015, He λ5876 and Hα. The model matches the positions and profiles of all these lines. However, the strength of the synthetic He λ5876 π feature at $\sim$5840 Å is clearly too large compared to the data. A possible reason for this is indicated in Figure 3 in the Zeeman curves of the helium lines. Beyond a field of 20 MG, the tables by Kemic do not give helium line positions. For the case of Feige 7 where fields above this strength are encountered, we have linearly extrapolated the Zeeman curves. Consider the case where this extrapolation shifts the wavelength of the He λ5876 π feature *less rapidly* than the line position actually does shift. The result would be absorption calculated over a range of wavelengths which is narrower than the actual absorption range. We would therefore expect a synthetic profile which was too deep compared to observations. It will be important to keep in mind this limitation associated with the calculation of helium line profiles in what follows. Nevertheless, Figure 5 shows us that a centered dipole field with polar strength 35 MG is an excellent starting point for our analysis of Feige 7.

4. ANALYSIS OF FEIGE 7 INTENSITY DATA

4.1. *Failure of the Centered Dipole Model*

The single observed property of Feige 7 which rules out a centered dipole model for the star is that the periods P_{spec} and P_{pol}, respectively associated with changes in its spectrum and circular polarization, are *equal* (L77), rather than having $P_{spec} = P_{pol}/2$. The photometric period, P_{phot}, of Feige 7 is also equal to P_{pol} (see also § 5). The intensity spectrum associated with a dipole field (centered or offset) is dependent only on the angle i (where $i \leq \pi$) between the observer's line of sight and the z-axis (dipole axis). We may write an expression for cos i as

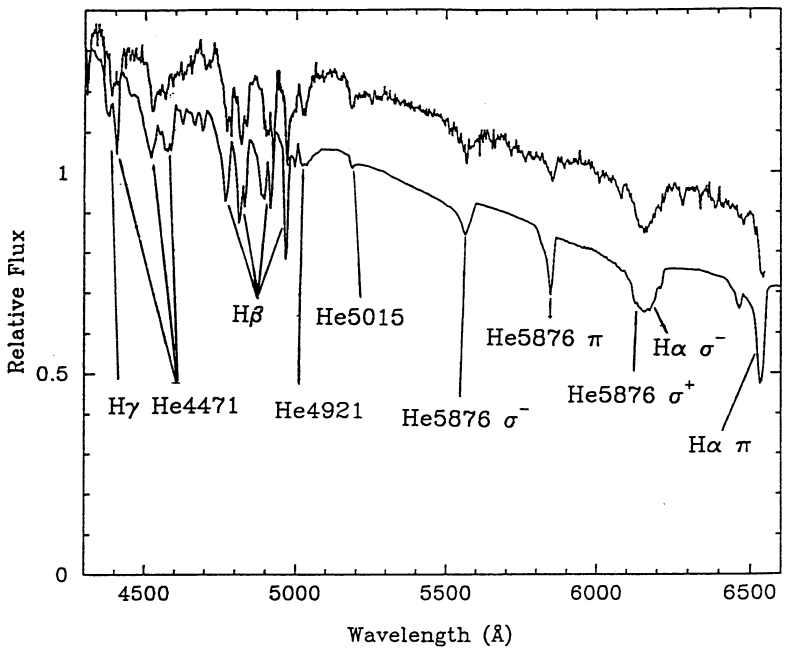

FIG. 5.—Comparison of one spectrum with a centered dipole model. The observed spectrum of Feige 7 at rotational phase $\Phi_{rot} = 0.038$. Below the observation is a synthetic spectrum associated with a model star with parameters $B_d = 35$ MG, $i = 90°$ and composition He:H = 100:1. The field is centered dipolar. Both model and observation are scaled to the same flux at 5300 Å, with the observation vertically shifted for comparison.

follows:

$$\cos i = \sin i_s \sin \theta_{dip} \cos 2\pi\delta + \cos i_s \cos \theta_{dip} . \quad (7)$$

Where i_s is the angle between the observer's direction and the white dwarf spin axis and θ_{dip} is the angle between the dipole axis and the spin axis. δ is the rotational phase, with $\delta = 0$ corresponding to the phase where the dipole points most closely to the direction of the observer (that is, the dipole direction lies in the plane of the observer's direction and the spin axis). For the case of a centered dipole model, $i = 90°$ presents a view of the field geometry that has no net component in the direction of the observer. This results in zero circular polarization.

Circular polarization is sensitive to mean field direction. In the case of Feige 7, the circular polarization varies approximately sinusoidally and symmetrically about a mean of zero (L77). This requires a symmetric variation in the angle i about a mean of 90°, and a dipole field which is centered or moderately offset ($a_z \lesssim 0.1$). In other words, if we look at equation (7), we require cos i to vary symmetrically about zero. Clearly, the two ways this may be achieved are, first, if $\cos i_s = 0$ and the observer views the spin axis at a right angle, or, second, if $\cos \theta_{dip} = 0$ and the dipole and spin axes are orthogonal. The former case requires no special orientation of the dipole and is referred to as the *sky rotator model* (since the spin axis lies in the plane of the observer's sky). The latter case requires no special viewing aspect for the observer and is referred to as the *orthogonal rotator model*. Equation (7) tells us that during one rotational cycle, a sky rotator with $\theta_{dip} = \alpha$ and an orthogonal rotator with $i_s = \alpha$ will be viewed over precisely *equal* ranges in angle i. Therefore, two such models *cannot* be distinguished through analysis of the observations.

Now consider two phases of an orthogonal rotator or a sky rotator where $i = \beta$ ($0 \leq \beta \leq \pi/2$) and $i = \pi - \beta$. These phases are separated by half a period and have the same magnitude but opposite sign for cos i. The sign of cos i indicates the direction in which the dipole is pointing relative to the observer's direction and thus determines the magnitude and sign of circular polarization. However, it is the absolute value of cos i which indicates the smallest angle between the z-axis direction and the observer's direction. For a centered dipole, it is this angle which determines the appearance of the Zeeman intensity spectrum (since the dipole is equidistant from the observer at all phases). It follows that the two phases considered will have identical Zeeman spectra but differing circular polarizations.

This means that, for a star with a centered dipole field whose circular polarization varies symmetrically about zero, there will be two cycles of variation in the intensity spectrum for every one cycle of variation in continuum circular polarization.

Since the circular polarization and spectral periods of Feige 7 are equal, we are forced to discount a centered dipole field as a possibility in modeling this star. Offset dipole models have been shown to be useful in simulating the fields of magnetic white dwarfs whose spectra cannot be interpreted using centered dipoles (Achilleos & Wickramasinghe 1989). A rotating offset dipole field will retain the approximately symmetric variation in circular polarization seen by L77 for adequately small offsets. We should therefore consider the question of whether or not such a field can reproduce the variation in line strengths and positions in Feige 7.

We conclude this section by making a comparison, in Figure 6, between a set of centered dipole models and the data of Figure 3. The models have a polar field $B_d = 35$ MG, an effective temperature $T_{eff} = 20{,}000$ K and a uniform atmospheric composition with He:H = 100:1 being the number density ratio of helium to hydrogen.

We see that, within the realm of the centered dipole models, viewing angles larger than 45° are required to reproduce the Zeeman complexes at $\lambda\lambda$4700–5100 with the closest possible

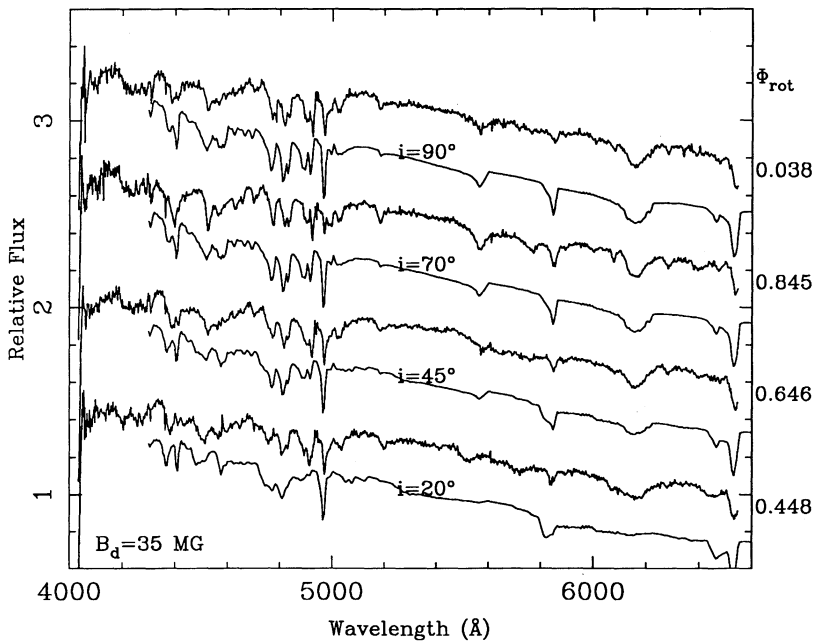

FIG. 6.—Centered dipole models labeled with viewing angle i plotted among four representative spectra of Feige 7. Models and data are scaled to the same flux at 5300 Å and vertically shifted. The observed variations in the Zeeman absorption patterns cannot be entirely reproduced using a centered dipole field.

match to profile shapes and relative strengths. The same range in angles is required to simulate the persistence of the Zeeman lines redward of λ5000. This is because values of i smaller than 45° lead to larger effective field spreads which broaden the Hα and He λ5876 σ components to the point where they are no longer seen.

Consider the variations seen in the Hα/He λ5876 absorption trough at 6150 Å. This feature is observed to broaden significantly in the phase range $\Phi_{rot} = 0.25$–0.60. It becomes narrower and its central depth increases by a factor of roughly 1.5 for the phase range $\Phi_{rot} = 0.70$–0.95. The centered dipole models with angles larger than 45° do not reproduce this behavior. Because hydrogen is the dominant element which forms this line (see Fig. 7), the corresponding synthetic profiles are mostly based on accurate Zeeman shifts.

We also note that the shift of $\sim$30 Å seen in the He λ5876 feature close to 5560 Å is not reproduced by the centered dipole models. The Zeeman shifts for this feature are not known above a field of 20 MG, however, and it is possible that a Zeeman curve which moves blueward more rapidly than our linear extrapolation would give rise to a synthetic profile which matches the shift observed.

The separation between the pair of Hβ lines centered at 4800 Å is observed to vary by $\sim$15 Å during the rotational period of Feige 7. The centered dipole models with large i also do not show this behavior. The forest of Hβ lines and the absorption trough at 6150 Å are our principal diagnostics of field structure and composition, since synthetic profiles we calculate in an attempt to match their behavior are mostly based on Zeeman shifts which are well known for the full range of surface magnetic fields in Feige 7.

We now consider the photometric variations of Feige 7, which were reported in § 3. The photometric period P_{phot} is equal to the polarimetric period P_{pol} due to the unequal maxima seen in the light curve, each of which appears and subsides over one half-cycle. These photometric variations rule

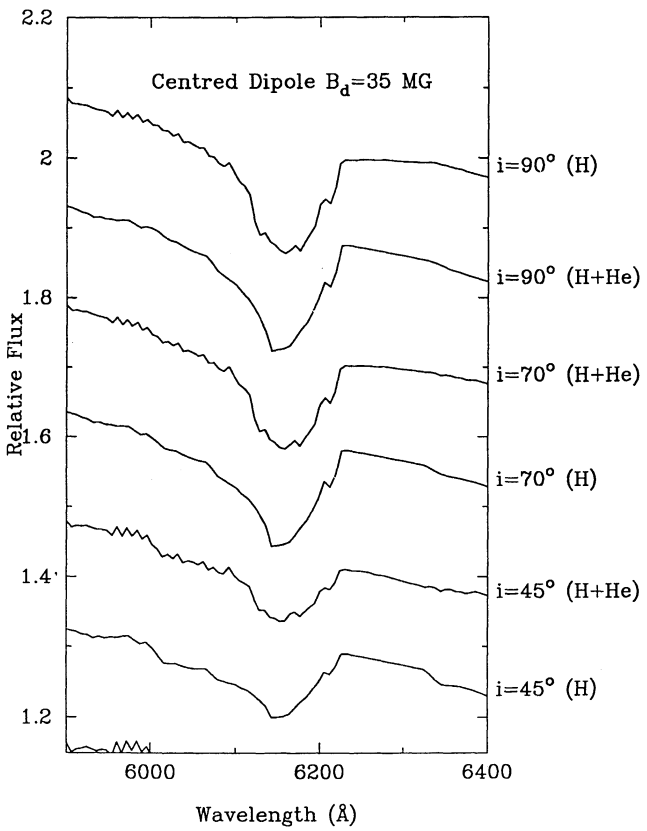

FIG. 7.—Synthetic trough at $\lambda\lambda$6050–6220 calculated using a pure Hydrogen atmosphere (H) and a mixed atmosphere with He:H = 100:1 (H + He). Each profile is labeled with viewing angle i. The figure shows that hydrogen is the dominant line-forming element for this absorption complex.

out an orthogonal or sky rotator with a centered dipole field. This is because, as was discussed above, the intensity predicted by such models varies with a period equal to half of the associated polarimetric period. If we consider the photometry alone and independently of the symmetry in the polarization curve, we cannot rule out the possibility of a centered dipole rotator which is neither an orthogonal nor sky rotator. It is the symmetry in the polarimetric variations which is the predicted signature of these two types of model, and it is the equality of the spectroscopic, photometric, and polarimetric periods that excludes centered dipole fields.

4.2. *The Offset Dipole Model*

In this section, we examine a series of models with offset dipole fields in order to see whether or not the variations in the intensity spectra of Feige 7 can be interpreted as the result of viewing an offset dipole at different angles. We calculated a grid of models with offsets of up to $a_z = 0.2$ and dipole strengths between 30 and 40 MG, spanning a range of viewing angles between $i = 40°$ and $i = 140°$. Visual comparisons with the data revealed that the best match to the observed variation in the Hα/He λ5876 trough at λ6150 and the blue Hβ forest of lines was obtained using $B_d = 35$ MG (identical to the centered dipole approximation) and $a_z = 0.15$. We also found that, if we assumed an atmosphere of homogeneous composition for Feige 7, then we require *different* ratios of He:H to match the intensity spectrum at different phases.

We compare models and observational data in Figure 8. We compare the intensity spectrum at phase $\Phi_{rot} = 0.448$ with three models viewed at $i = 140°$, differing only in their atmospheric composition. Our two principal features—the Hα/He λ5876 trough and the Hβ forest—match the observations for a composition between He:H = 100:1 and 500:1. Interestingly, the He λ5876 σ^- feature is now blueshifted relative to its location in the centered dipole models. This location also matches the observed line position. In the comparisons we make hereafter, the largest errors in dipole strength B_d and viewing angle i are about 2 MG and 10°–15°, respectively.

It is important to note that the $i = 140°$ model yields the broadest Hα/He λ5876 trough. This seems peculiar in light of

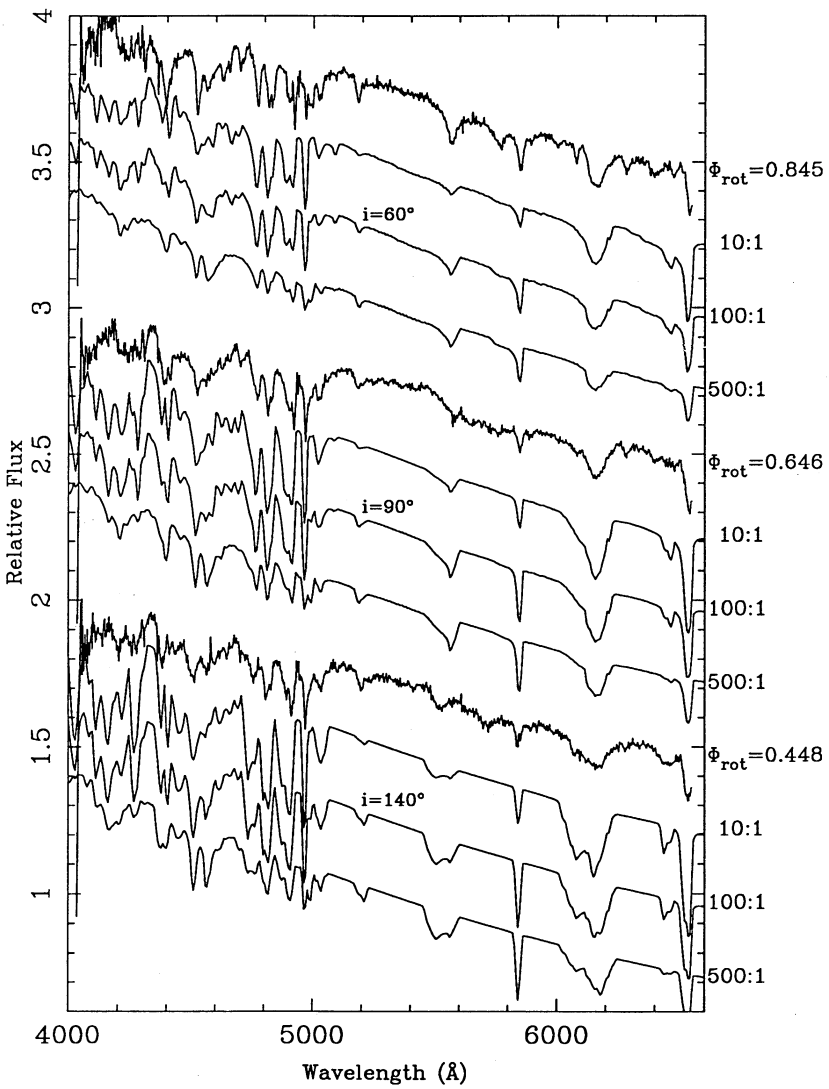

FIG. 8.—Offset dipole models plotted with three observed spectra. Viewing angle i is shown. The ratios on the right vertical axis show He:H for the model atmosphere used in each case. Models and data ($B_d = 35$ MG, $a_z = 0.15$) are scaled to the same flux at 5300 Å and vertically shifted.

the fact that this view of the offset dipole reveals the most uniform model field distribution (since the dipole is furthest from the observer at this viewing angle). Normally, Zeeman features generally become narrower and deeper with more uniform surface fields, reflecting the smaller range of wavelengths over which absorption occurs (Achilleos & Wickramasinghe 1989 have illustrated this point). All the pure hydrogen Zeeman lines become deeper as i goes from 60° to 140° and the spread in surface fields decreases.

However, we do not see this behavior in the Hα/He λ5876 trough or the He λ5876 σ^- feature. The reason for this lies in the Zeeman curves corresponding to these lines in Figure 3. We see that the Hα/He λ5876 trough is formed from two sets of Zeeman features. The Hα σ^- components and the He λ5876 σ^+ components. Both of these and the He λ5876 σ^- components are the Zeeman lines whose positions shift most rapidly with field.

Consider the He λ5876 σ^- lines and the view $i = 60°$ of our offset dipole. If we look at Figure 2, we see that a line absorption will occur mostly at a field strength close to equatorial (17.5–20 MG in our model). The contribution to the line absorption, as measured by the projected surface area, rapidly decreases as we move to higher fields and bluer wavelengths, corresponding to polar magnetic latitudes (regions closer to the pole). This explains the shape of the synthetic $i = 60°$ profiles. A steep redward "edge" (absorption from regions close to the magnetic equator) becoming shallower with bluer wavelength.

Now consider the $i = 140°$ viewing aspect. Here we are viewing the other hemisphere of the model star. The field now changes much less rapidly with magnetic latitude. This means that as we move closer to the pole from the equator we experience absorption which is confined to a narrower range of fields and wavelengths than for the $i = 60°$ case. In terms of synthetic profile shape, the $i = 60°$ trail of blue absorption becomes more concentrated and shifts closer to the red edge, resulting in a line whose central wavelength is blueshifted. Similar reasoning explains the broadening of the Hα/He λ5876 trough. The red edge in this case remains strong at all viewing angles because the feature is formed from two sets of oppositely moving σ components. A strong red edge is seen at all views thanks to the contribution for the Hα components.

In Figure 8, we identify the closely matching spectra at $\Phi_{rot} = 0.646$ and $\Phi_{rot} = 0.038$ as offset dipole fields viewed at $i \sim 90°$. The composition He:H = 100:1 gives the best match to the line strengths in the Hβ forest, the shape and strength of the Hα/He λ5876 trough and the position of the He λ5876 σ^- feature.

In Figure 8, we look at the spectrum taken at $\Phi_{rot} = 0.845$. It is about 0.2 phase units away from the spectra associated with $i = 90°$. For an orthogonal rotator with $i_s = \alpha$ or a sky rotator with $\theta_{dip} = \alpha$, we see from equation (7) that the angle i varies between $|\alpha - 90°|(\cos 2\pi\delta = 1)$ and $\alpha + 90°(\cos 2\pi\delta = -1)$. Between these extremes, $\cos 2\pi\delta = 0$ and $i = 90°$. Our models indicate that i at one of the "extreme" phases is 120°–140°. For an orthogonal or sky rotator, the other extreme angle would be 40°–60°. We see that an angle $i = 60°$ matches the Hβ line strengths and Hα/He λ5876 trough profile in Figure 8 if we take a composition between He:H = 10:1 and He:H = 100:1.

An offset dipolar field, according to our models, is a much improved representation of the magnetic field in Feige 7. Using an offset of $a_z = 0.15$ and a dipole strength of $B_d = 35$ MG, we can reproduce many of the variations in the intensity spectra (for features whose Zeeman shifts are accurate over the entire field range). These variations arise from viewing the dipole at different angles as the star rotates. We require different He:H ratios at different phases (assuming a homogeneous surface composition). The phases associated with largest i (120°–140°) require "helium-rich" atmospheres ($100 <$ He:H < 500). Phases for which $i \sim 90°$ are best matched by "helium-intermediate" atmospheres (He:H ~ 100:1) while those phases which are best matched by angles $i = 40°$–$60°$ also require "helium-poor" atmospheres ($10 <$ He:H < 100). The principal effect of increasing the hydrogen concentration in our model atmospheres is an increase in the continuous opacity and a weakening of the pure He lines. Indeed, all pure He features are weaker in observed spectrum at $\Phi_{rot} = 0.448$ (associated with the $i = 140°$ models) than in the spectrum at $\Phi_{rot} = 0.845$ (associated with the $i = 60°$ models). This tells us that, within the framework of an offset dipole field, Feige 7 shows evidence for variations in composition across its surface. This possibility was also noted by L77 in their consideration of the red Zeeman lines and their relative strengths.

4.3. *The Cap Model*

We now consider the question of whether we can construct models for Feige 7 with a definite prescription of surface abundance patterns that will improve and extend the agreement between observed and theoretical intensity spectra. For this purpose, we retained our model field structure of z-offset dipole. The principal reason for this was to try and preserve the property of a rotating offset dipole related to circular polarization.

L77's broad-band circular polarization measurements of Feige 7 provide an important constraint for our modeling. Their measurements are approximately described by a sinusoidal variation in circular polarization with amplitude ~0.4% about a mean of ~0%. An orthogonal/sky rotator model employing a z-offset dipole is a simple means of reproducing a polarization variation that is approximately sinusoidal (provided the offset is not too large). Moreover, the dipole offset generates variations in polarization and intensity with identical periods, in agreement with what is observed.

Using our favored field geometry, we generated a grid of models whose abundances varied over the surface of the model star. The most simple kind of abundance variation is homogeneous surface "patches" of different composition. Our first attempts at modeling the abundance variation employed patches whose composition could be pure hydrogen, pure helium, or the intermediate composition I with He:H = 100:1. The shape of these patches, for simplicity, took the form of caps centered on one of the magnetic poles and covering the stellar surface up to some limiting magnetic latitude.

Visual comparison with the observations was adequate for distinguishing which set of cap models provided the best match to the data. In Figure 9, we show our three representative spectral observations plotted along with synthetic spectra associated with 12 different cap models, which include those models which fit the data most closely. For each model, the extent of the cap from the strongest magnetic pole ($\Delta\theta_{cap}$) is shown and the composition of the cap is also indicated. The rest of the model star's atmosphere was assumed to be pure helium. We now compare theory and observation for the three different views $i = 60°$, 90°, and 140°. In the context of the cap models, it was these viewing angles (to within 10°–15°) that again provided the best visual comparison to the data.

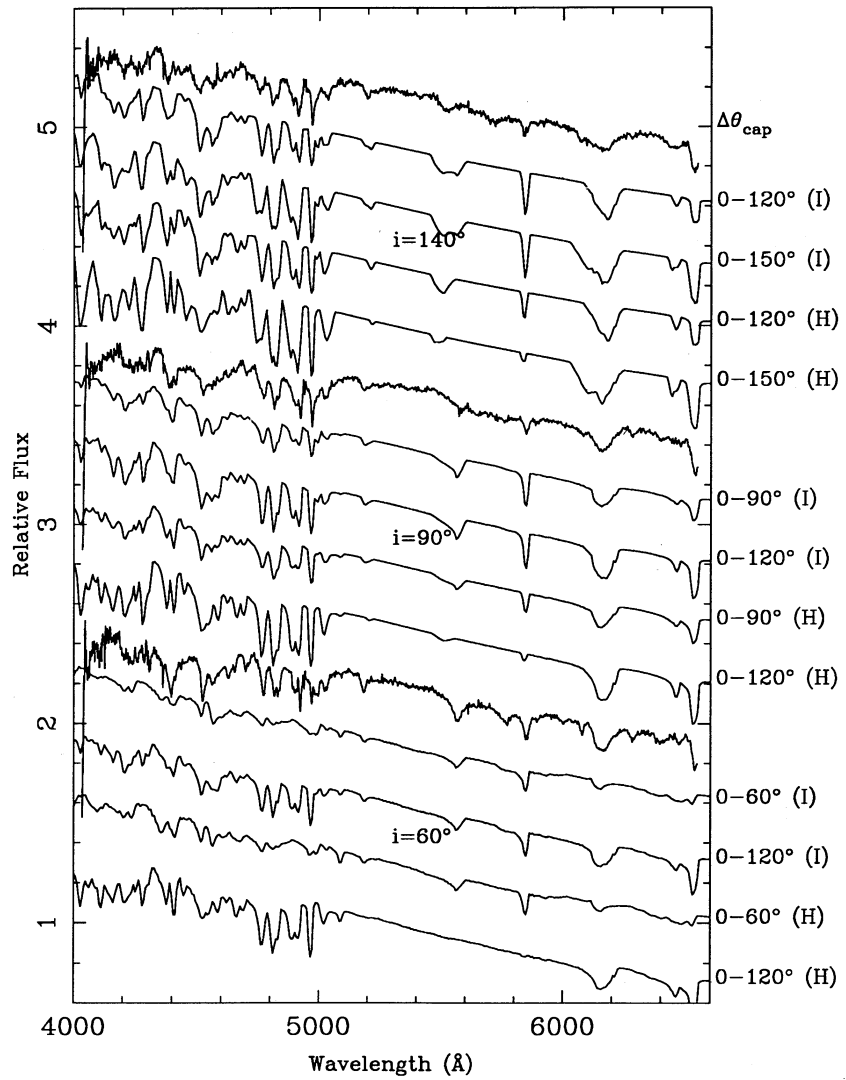

FIG. 9.—Cap models. Models are plotted along with the three spectra used in Fig. 8. The viewing angle i, cap size $\Delta\theta_{cap}$ and cap composition [I (He:H = 100:1) or H (pure hydrogen)] are also shown. Models and data are scaled to the same flux at 5300 Å and vertically shifted.

Consider the case $i = 140°$. The $\Delta\theta_{cap} = 120°$ models provide the best Hβ line strengths (although these are still slightly too strong in comparison with those observed). Of these, the pure H cap shows a better shape for the He λ5876 σ^- feature and relative strength of the He λ5015 and He λ5876 lines. The Hα/He λ5876 synthetic trough is too strong for all models shown, but is of the correct breadth for the $\Delta\theta_{cap} = 150°$ models. The closest overall fit is achieved with a pure H cap extending from the strongest pole to a magnetic latitude θ between 120° and 150°. A definite improvement for this view has been attained in comparison with the homogeneous composition models of Figure 8, mainly in terms of the strengths of the pure He features.

Consider the case $i = 90°$. A cap size between 90° and 120° provides an excellent match to the strengths and positions of the lines in the Hβ forest and also to the absorption pattern due to He λ4471 and Hγ blueward of 4700 Å. The pure H cap models clearly show an improved relative strength of the series of all features redward of 5100 Å. There is a marginal improvement in the appearance of these lines over those of homogeneous composition models of best fit (Fig. 8). Our best-fitting model for this phase is a pure H cap extending from $\theta = 0°$ (strongest pole) down to somewhere between 90° and 120°.

Consider the case $i = 60°$. The models with cap sizes closest to 120° provided adequately strong Hβ forests. The pure H cap models, however, lost all trace of their red pure He features at this cap size. The closest fit is obtained with a cap of composition I extending to $\theta \sim 120°$. We note that the He λ5876 σ^- synthetic feature remains too weak in comparison with the observed line. The relative strengths of the He λ5876 π feature and the He λ5876/Hα trough are well matched to those observed. For $i = 60°$, we do not see magnetic latitudes beyond $\theta = 150°$. This is why the best-fitting cap and homogeneous composition models appear so similar (Fig. 8).

Although we have found cap models which provide agreement with most of the observed absorption lines, we require caps of different sizes and compositions depending on the phase of the star being viewed. Qualitatively speaking, the complete model we seek must satisfy the following constraints, revealed by the cap models of best fit:

1. The $i = 60°$ view must be dominated by composition I (He:H = 100:1).

2. A region with a larger concentration of hydrogen must be seen at $i = 90°$.

3. A region with about the same H concentration, but whose effective area is larger, must be viewed at $i = 140°$.

Let us take all of these features into consideration and keep as close as possible to the idea of simple caps to represent surface abundance gradients and discontinuities. We see that a *ring* of pure hydrogen extending between $\theta \sim 100°$ and a larger magnetic latitude, and bordered by regions of differing composition is the simplest way to explain the entire phase range of observations. We note that an H cap of a size $\sim 150°$ does not fit the phases $i = 90°$ and $i = 140°$ because the pure He features are too weak and the pure H features too strong. A ring of pure H as described above, bordered by pure He at the weak pole may alleviate this problem. This is because such a model keeps much of the surface area contributing to the H lines at these phases, and the introduction of a weak pole He cap reduces the H line strengths and enhances He line strengths. We explore such models in the next section.

4.4. *The Ring Model*

Our experiments with pure H ring models resulted in a set of six models for most closely simulating the variations of the spectral lines of Feige 7. For convenience, we refer to these models by the letters below denoting their abundance geometries. The H ring covers magnetic latitudes described by the range in the latitude angle θ. The composition of the region outside the H ring is given after the ring size:

Model A: $100° \leq \theta \leq 160°$ (Composition I outside)

Model *B*: $100° \leq \theta \leq 140°$ (Composition I outside)

Model C: $100° \leq \theta \leq 120°$ (Composition I outside)

Model D: $100° \leq \theta \leq 160°$ (Composition pure He outside)

Model E: $100° \leq \theta \leq 140°$ (Composition pure He outside)

Model F: $100° \leq \theta \leq 120°$ (Composition pure He outside).

In Figure 10, we show the six ring models described above calculated at viewing angles $i = 60°$, $i = 90°$, and $i = 140°$. For these three phases, we have also plotted the representative intensity data. We now outline our best-fitting models and any improvement they show compared to the cap models of best fit described above.

For the $i = 60°$ case, the H ring makes no significant contribution to the observed spectrum, and the ring models with backgrounds of composition I (A, B, and C) give a fit to the data of the same quality as the cap model of best fit (composition I, $\Delta\theta_{cap} \sim 120°$). Models D, E, and F, having pure He backgrounds, do not generate adequately deep H Zeeman lines to fit the spectrum. We note that the He $\lambda 5876$ π profile contains a hint of absorption in the form of a shallow blue "shoulder" accompanying the deeper redward edge. This blue part of the profile is due to absorption at the highest fields presented to the observer. This indicates that the unidentified Zeeman component seen at ~ 5760 Å in the data may be a helium Zeeman π feature, formed in a peculiar high-field region or "spot" superposed on the basic dipole. At this stage, such a suggestion is purely conjecture.

Consider the $i = 90°$ case. The red Zeeman lines ($\lambda\lambda 5300$–

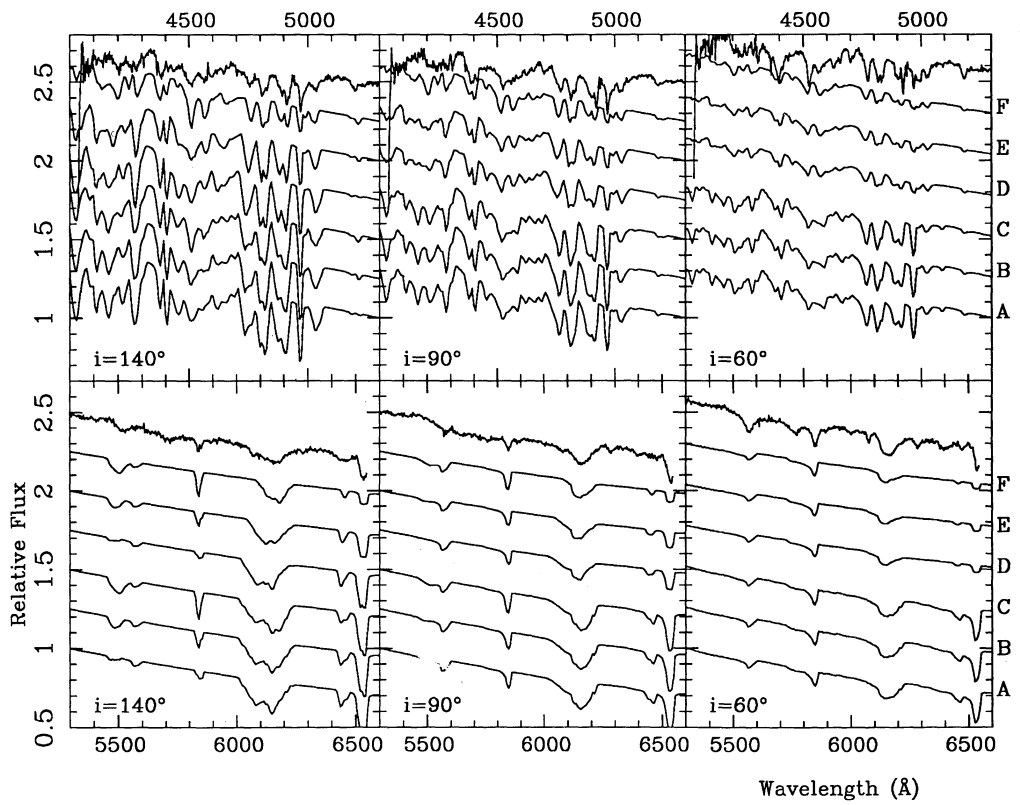

FIG. 10.—Models utilizing a surface "ring" of pure hydrogen. Models are shown beneath the blue (*upper plots*) and red (*lower plots*) regions of the observations from Fig. 9. The viewing angle i for each set of models is shown. Letters on the right vertical axis denote the abundance geometry of the six models shown in each panel, according to the code described in the text. Models and data are scaled to the same flux at 5300 Å and vertically shifted.

6600) have their strengths and profile shapes best reproduced by models D and E. Neither model provides a very good match to the blue Hβ forest in terms of the positions and relative strengths of all the lines in the range 4700–5100 Å. Models A and B show some improvement in this region but the synthetic He λ5876/Hα trough has a shape which is now in slightly poorer agreement with its observed counterpart. Taken separately, these ring models do not significantly improve upon the cap model of best fit. A model which combines the two in the form of compositions pure He and I on different sides of the ring would provide a fit equally good and probably superior.

Consider the $i = 140°$ case. A model with ring size between those of Models E and F would provide synthetic red Zeeman features whose relative strengths and profile shapes are clearly superior in matching the data than those of the best-fitting cap model. This type of ring model would also match the strengths and positions of the lines in the blue part of the spectrum dominated by hydrogen absorption.

The above considerations support a model for Feige 7 with a pure hydrogen ring spanning a range ~100°–130° in magnetic latitude. The model has a pure helium composition on the side of the weak pole (23 MG) and a composition with hydrogen and helium in the ratio He:H = 100:1 on the side of the strong pole (57 MG). We emphasize that this model is the result of experiments done under the assumption of ring- and cap-shaped "patches" of different composition. These compositions in turn were restricted to three possibilities (pure H, pure He, He:H = 100:1). It is impossible to explore the full range of possible model abundance distributions without imposing such simplifications.

As a result, it is not surprising that we cannot claim uniqueness for the above "ring" model. However, we have established the existence of abundance gradients on the surface of Feige 7 through our modeling. Furthermore, our best-fitting models all support a global abundance variation in which the surface regions close to the magnetic equator are hydrogen-rich and those closer to the magnetic poles are helium-rich (He:H $\gtrsim$ 100). It is therefore reasonable to suppose that the true surface abundance pattern of Feige 7 is in qualitative agreement with this description.

5. POLARIMETRIC AND PHOTOMETRIC VARIABILITY

As we have mentioned, any model for Feige 7 must reproduce the polarization variations observed for the star, as well as mimic the change seen in the Zeeman absorption spectra. The broad-band circular polarization of Feige 7 follows an approximately sinusoidal variation. L77's sinusoid of best fit to their polarimetric data has an amplitude of 0.4% and a period identical to Feige 7's rotational period (131.606 minutes = 7896.36 s). A further constraint for possible models is the photometric variability described in § 3.

Let us now investigate our ring models of best fit for Feige 7 and see how well they agree with respect to the polarimetric and photometric variations described above. To obtain a "white-light" polarization corresponding to L77's measurement, we calculated the mean circular polarization over a wavelength range λλ4000–7500 for each of the ring models. This was done by weighting the circular polarization at each wavelength by the intensity, adding these weighted polarizations, and then dividing by the total intensity in the entire wavelength range from 4000 to 7500 Å.

To obtain a synthetic V-magnitude, we multiplied each model by a response function corresponding to the V filter used in the observations. We then integrated the intensity which remained. The result, I, was converted into a magnitude equal to $-2.5 \log (I)$ without regard to zero point. These numbers are not supposed to simulate the apparent magnitude of Feige 7. They indicate the variation in V-magnitude due to rotation of the ring models.

Table 1 lists the synthetic broad-band circular polarization and V-magnitude for each of the ring models in Figure 10. We see that a change in viewing angle, keeping a fixed abundance geometry, generates only small variations in V (the largest variation is 0.07 mag for Model D, which is in good agreement with the observations). Now consider the change in going from Model A, for example, viewed at 60° to model D viewed at 90° to model E or F viewed at 140°. The change in V is between 0.1 and 0.14, in good agreement with the observations. The models required to effect this change correspond to the "composite" ring model described at the end of § 4.4. Evidently, the change in continuum opacity due to abundance gradients or discontinuities of this model viewed at different angles causes variations in V similar in magnitude to those observed.

The midpoint of the first integration in the V light curve occurs at HJD 2447805.686879, which corresponds to a phase 0.094, using the ephemeris from L77. This point occurs during a minimum in the V light. However, our model for Feige 7 requires the star to be viewed at angles close to $i = 90°$ at phases close to zero. Consider the viewing sequence going from Model A at $i = 60°$ to Model D at $i = 90°$ to Model E at $i = 140°$. The respective synthetic magnitudes are −0.0329, 0.0851, and 0.0730. The $i = 90°$ view therefore yields the faintest V light. This is an example of a viewing sequence which satisfies the constraints of the abundance geometry required to simulate the variations observed in the intensity spectra and also the viewing geometry indicated by the timing of the photometric variations (although this latter agreement is qualitative). The detailed shape of the photometric curves of Feige 7 may shed more light in the future on the issue of its surface abundance patterns.

Varying the viewing angle for each of the six ring models also causes a change in the broad-band circular polarization. The amplitude of this variation, from Table 1, is between 0.7%

TABLE 1

RING MODELS

Model	Viewing Angle i	V-Magnitude	$\langle V/I \rangle_{4000-7500}$
A	60°	−0.0329	−1.2520%
A	90	−0.0247	−0.3558
A	140	−0.0056	0.8510
B	60	−0.03310	−1.2520
B	90	−0.0281	−0.3609
B	140	−0.0200	0.8672
C	60	−0.0355	−1.2562
C	90	−0.0355	−0.3554
C	140	−0.0353	0.8559
D	60	0.1148	−0.7912
D	90	0.0851	−0.1209
D	140	0.0437	0.8118
E	60	0.1149	−0.7915
E	90	0.0911	−0.1209
E	140	0.0730	0.8449
F	60	0.1184	−0.7923
F	90	0.1063	−0.0948
F	140	0.1051	0.9294

and 1.3%. These amplitudes are larger than L77's figure of 0.4%, but certainly the same order of magnitude. However, it should be noted that the observations of L77 were not corrected for the polarimeter response at different wavelengths. This means that their data show a smaller amplitude for circular polarization than the actual value. In light of this information, our synthetic amplitudes may be quite reasonable estimates of the polarization variations of Feige 7.

6. DISCUSSION

We have analyzed high-resolution spectral data for the magnetic white dwarf Feige 7. We performed this analysis using synthetic spectra generated by our models for such stars which incorporate realistic model atmospheres of varying composition. A study of the behavior of the Zeeman absorption line positions and profiles with time yielded a good approximation to the field geometry of Feige 7. This geometry was a dipole of strength 35 MG situated 0.15 white dwarf radii from the stellar center. This field structure is viewed at angles between $i = 50° \pm 10°$ and $130° \pm 10°$ to its magnetic axis of symmetry.

Further investigation of the observed strengths revealed evidence for composition changes across the surface of Feige 7. We attempted to map the surface abundance pattern of Feige 7 using a set of models with simplified abundance geometries. These geometries took the form of "caps" and "rings" of a homogeneous composition extending between lines of magnetic latitude. Within this framework, the best-fitting model for Feige 7's surface abundance pattern is as follows: a hydrogen-rich (or pure hydrogen) ring extending between latitudes $\sim 100°$ and $\sim 130°$ from the stronger magnetic pole. Outside this ring, on the side of the weak pole, is a helium-rich (or pure helium) region. The region on the side of the strong pole has a composition more rich in hydrogen (He:H = 100:1 for this region in the model). We show a diagram of this abundance model in Figure 11. Also shown are the magnetic field lines generated by the offset dipole in our model for Feige 7. The "cone" swept out by the observer's line of sight, relative to the white dwarf during its rotation, is also shown for an orthogonal rotator geometry (spin and dipole axes are separated by 90°). For a sky rotator, the viewing cone would actually be a circle in the plane perpendicular to the spin axis and the spin and dipole axes would be separated by an angle different from 90°.

We now address the question of the origin of such an abundance pattern. There are two possibilities to be considered. The first involves accretion of hydrogen onto a star whose atmosphere is originally dominated by helium. The second possibility is related to a picture of the evolution of surface abundances in white dwarfs and appeals to the efficient mixing processes which are claimed to occur in white dwarf atmospheres in certain regimes of temperature.

6.1. *An Accretion-Based Origin?*

Our model for Feige 7 points towards a hydrogen "ring" located close to the magnetic equator of the star. This model ideally is a close approximation to the true surface abundance geometry. We consider now the possibility that such a region of hydrogen may have originated from accretion of gas, either from a companion or from the interstellar medium. The former case would require Feige 7 to have been, at some stage in its life, the primary component of a binary system. We can safely assume that Feige 7 possessed a field very similar to its current one, in light of the results by Wendell, Van Horn, & Sargent

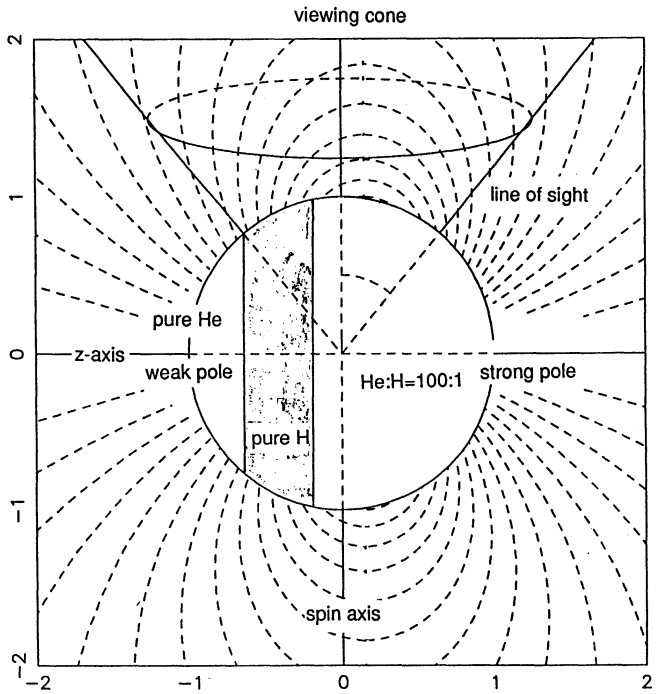

FIG. 11.—Abundance geometry model. A ring of hydrogen is located close to the magnetic equator. The weaker pole is covered by a helium cap and the stronger pole by a mixture of helium and hydrogen with He:H = 100:1 (number density ratio).

(1987). Their calculations for low-order eigenmodes of dipole and quadrupole fields in white dwarfs indicate that these field components decay on time scales greater than white dwarf cooling times. The cooling time for Feige 7 is of the order 10^8 yr (L77). Moreover, the field strengths in the atmosphere of Feige 7 ($\sim$25–50 MG) lie within the range of fields detected in the white dwarfs of AM Herculis binaries.

The surface field generated by our offset dipole model can be expressed using a combination of centered multipoles (see Appendix). The ratio of centered quadrupole to centered dipole in our field with offset $a_z = 0.15$ is given by $3a_z = 0.45$. The field of our model, then, is dominated by a centered dipole plus centered quadrupole combination. These components contribute approximately $\frac{2}{3}$ and $\frac{1}{3}$ of the total field, respectively. Figure 12 shows four different sections of the model field presented to the observer as rotation proceeds. Contours of field strength are shown in the plots of the visible disk of the model. It is evident that the views of the two magnetic poles present regions of very different field spread to the observer.

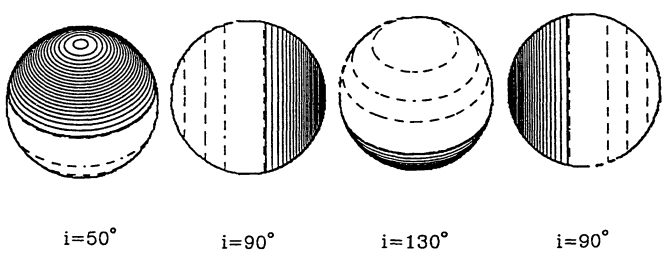

FIG. 12.—Views of the model field during rotation. Each view of the model star shows contours of equal field strength. The change in field strength between contours is the same for all views. Dotted and solid contours indicate field vectors at those positions pointing into and out of the stellar surface, respectively.

Can such a field accrete an equatorial ring of hydrogen? A binary with synchronized component stars and a strongly magnetic white dwarf primary is an AM Herculis system. The magnetic field of the white dwarf controls the accretion flow close to the star. Ionized accreting material is thought to couple onto the magnetic field lines at roughly the point where the ram pressure of the accretion flow is exceeded by the magnetic pressure of the field (Beuermann 1988 has an excellent review of accretion processes). Typically, the material couples on to the field at distances $r_{coup} \sim 10$–$30\ R_{wd}$ from the white dwarf, where R_{wd} is the white dwarf radius.

If we look at the field lines in Figure 11, we see that we require r_{coup} to be much smaller than this if accreted material is to follow field lines to a surface region close to the magnetic equator. The field lines emanating from the magnetic latitudes between 100° and 130°, corresponding to our H ring location, are associated with coupling regions located at $r_{coup} \leq \sim 2.4\ R_{wd}$. Any material being accreted on to the hydrogen ring must therefore penetrate extremely deeply into the white dwarf magnetosphere. Neutral material may freely cross field lines before it is ionized. However, it is not likely that any of the accreting material in AM Herculis systems resists ionization all the way down to these small values of r_{coup}.

Accretion from the interstellar medium by the magnetic white dwarf does not help in acquiring a small r_{coup}. An 11,000 K white dwarf moving at 50 km s^{-1} through a medium with $n_H = 10^2$ cm^{-3} keeps hydrogen ionized out to $\sim 10^4\ R_{wd}$ (Alcock & Illarionov 1980). A mechanism which would perhaps help accreted material couple to the field at small values of r_{coup} is the "screening" of material from the magnetic field by currents flowing in it (Beuermann 1988; Lamb & Melia 1988).

An accretion scenario thus encounters difficulties in explaining the small coupling distance required to produce an accreted equatorial H ring. For a dipole field, the accretion which occurs from a companion star or from the interstellar medium onto a magnetic white dwarf follows field lines which terminate at the surface of the white dwarf preferentially close to the magnetic poles. We consider, in the next part of our discussion, an alternative possibility for the origin of the abundance pattern in Feige 7.

6.2. *A Mixing-Based Origin?*

One current picture of white dwarf evolution makes the following claim. White dwarfs with adequately thin external layers of hydrogen ($\lesssim 10^{-15}\ M_\odot$) covering a deeper helium layer are subject to convective instability of the helium zone once the star becomes cooler than $\sim$30,000 K (effective temperature) (Fontaine & Wesemael 1987; Liebert, Fontaine, & Wesemael 1987). Below 30,000 K, the helium layer mixes with hydrogen from above, turning a DA into a DB white dwarf. This mixing is proposed to explain the fact that about $\frac{1}{4}$ of all white dwarfs in the temperature interval 12,000–30,000 K are DB, while no DB or DO stars are known in the interval 30,000–45,000 K.

The mass of the helium convection zone is about $10^{-6}\ M_\odot$. This results in a hydrogen abundance (by mass) of 10^{-5}–10^{-10} in the atmospheres of these DB stars after complete mixing has occurred (Koester 1987). The hydrogen mass abundance in our composite ring model for Feige 7 varies from about zero near the weak pole to about 1.00 in the H ring to about 0.0025 near the strong pole. The pure helium region could be a result of the mixing episode described above.

Why, then, did this mixing not occur over the entire surface of Feige 7, as in other DB stars? The answer lies in the magnetic field of Feige 7. The motions of stellar material in the presence of a magnetic field are confined along the direction of field lines (see Cowling 1965). L77 showed that the field in Feige 7 could conceivably suppress convection across field lines.

We would therefore expect any H-rich regions where mixing was inefficient to be located at positions where the field lines have a large component tangential to the stellar surface. The hydrogen ring of our model is, indeed, in such a position. The field lines at both poles are in an approximately radial direction, so we expect efficient mixing at the poles, resulting in pure He regions or, perhaps, He-rich regions containing some hydrogen accreted onto the pole from the interstellar medium. This is also consistent with our "composite" ring model. A mixing scenario with magnetism included is thus capable of explaining a surface abundance pattern in qualitative agreement with our model.

We should also note that some 20% of the general class of DB stars (that is, those without detected magnetic fields) show weak Balmer lines and trace abundances of hydrogen (Shipman, Liebert, & Green 1987). Again, the two alternative scenarios of accretion and convective mixing are discussed as possible origins of the trace hydrogen abundances. The discovery of weak Ca II lines in several of these stars (Sion, Aannestad, & Kenyon 1988) strengthens the case for accretion, since calcium could not be dredged up from the deep interior.

None of these DBA stars has a derived hydrogen abundance higher than the order of $10^{-4}(n_H/n_{He})$, while Feige 7 has surface regions with the order 10^{-2} and, if our analysis is correct, even higher. Thus, it would appear at face value that the appearance of hydrogen on the surface of this star with a $\sim$35 MG magnetic field has a much different origin than that for the normal DBA stars. However, all analyses of DBA stars have assumed that the H/He abundance is uniform across the stellar surfaces, whereas this may not necessarily be the case. Moreover, the absence of polarization or Zeeman features in photometric and spectrophotometric observations of the normal stars is sufficient to limit any existing fields on the surface only to the order 10^6 G in all legitimate DB stars except GD 358 for which limits are summarized in Angel, Borra, & Landstreet (1981). GD 358 lacks a longitudinal field larger than about 4×10^4 G, corresponding to a surface field strength no larger than the order 10^5 G. The possibility thus cannot be excluded that this subset of DB stars consists of those with inhomogeneous surface compositions, caused by the presence of moderate magnetic fields. Such objects would be the low-field "cousins" of Feige 7.

J. L. acknowledges support from the National Science Foundation through grant AST 91-45162. D. T. W. is grateful to Peter Strittmatter, Director of Steward Observatory, for financial support for his sabbatical visit during which time this work was commenced. N. A. acknowledges financial support from the Australian Department of Industry, Technology, and Commerce, and is grateful to François Wesemael for additional reading of the text and comments.

APPENDIX

FIELD POTENTIAL OF AN OFFSET DIPOLE

We seek the mixture of centered magnetic multipoles that generates a field equivalent to that of a dipole, displaced a_z units along its axis of symmetry.

The fields of multipoles can be expressed as the gradients of scalar potentials. These potentials are as follows for three different centered multipoles (see also Martin & Wickramasinghe 1984):

$$\Phi_1 = \frac{B_d}{2}\frac{\cos\theta}{r^2} \qquad \text{(Centered Dipole)} \tag{8}$$

$$\Phi_2 = \frac{B_d}{3}\frac{(-3/2)\cos^2\theta - 1/2}{r^3} \qquad \text{(Centered Quadrupole)} \tag{9}$$

$$\Phi_3 = \frac{B_d}{4}\frac{(5/2)\cos^3\theta - (3/2)\cos^2\theta}{r^4}, \qquad \text{(Centered Octupole)} \tag{10}$$

where r denotes the distance from the center ($r = 1$ is the star's surface), B_d is the multipole strength, and θ is the magnetic latitude—the angle between the magnetic axis of symmetry and the position vector of the point in question. Equations (8), (9), and (10) follow the general form for multipole potentials:

$$\Phi_n = \frac{B_d}{n+1}\frac{P_n(\cos\theta)}{r^{n+1}}, \tag{11}$$

where P_n is the nth Legendre polynomial. The potential associated with a centered dipole may be rewritten in terms of Cartesian coordinates. We define $z = r\cos\theta$ and $r^2 = x^2 + y^2 + z^2$ and obtain

$$\Phi_1 = \frac{B_d}{2}\frac{z}{(x^2 + y^2 + z^2)^{3/2}}. \tag{12}$$

To obtain the potential of a dipole displaced by a_z stellar radii along its axis of symmetry, we replace z in the above equation by $z - a_z$, and replace $r^2 = x^2 + y^2 + z^2$ by $x^2 + y^2 + (z - a_z)^2$:

$$\Phi_{\rm off} = \frac{B_d}{2}\frac{z - a_z}{[x^2 + y^2 + (z - a_z)^2]^{3/2}} = \frac{B_d}{2r^2}\frac{\cos\theta - (a_z/r)}{[1 - 2(a_z/r)\cos\theta + (a_z/r)^2]^{3/2}}. \tag{13}$$

The bracketed denominator may be expanded in terms of Legendre polynomials to yield the following expression:

$$\Phi_{\rm off} = \frac{B_d}{2r^2}\left(\cos\theta - \frac{a_z}{r}\right)\left[\sum_{n=0}^{\infty} P_n(\cos\theta)\left(\frac{a_z}{r}\right)^n\right]^3. \tag{14}$$

If we consider regions where $(a_z/r) \ll 1$ and retain terms with powers of a_z/r less than or equal to 2, our expression becomes

$$\Phi_{\rm off} = \frac{B_d}{2r^2}\left(\cos\theta - \frac{a_z}{r}\right)\left[P_0^3 + 3P_0^2 P_1\frac{a_z}{r} + (3P_0 P_1^2 + 3P_2 P_0^2)\left(\frac{a_z}{r}\right)^2\right]. \tag{15}$$

The argument of the Legendre polynomials in the above equation is $\cos\theta$. The following are the explicit forms for the first three P_n.

$$P_0(x) = 1 \tag{16}$$

$$P_1(x) = x \tag{17}$$

$$P_2(x) = \tfrac{1}{2}(3x^2 - 1). \tag{18}$$

If we substitute equations (16) through (18) into equation (15) and make use of equations (8) through (10), some manipulation yields the following expansion for the offset dipole potential:

$$\Phi_{\rm off} = \Phi_1 + 3a_z\Phi_2 + 6a_z^2\Phi_3. \tag{19}$$

These are the first three terms which express the offset dipole potential as the sum of centered multipoles.

REFERENCES

Achilleos, N., & Wickramasinghe, D. T. 1989, ApJ, 346, 444
Alcock, C., & Illarionov, A. 1980, ApJ, 235, 541
Angel, J. R. P., Borra, E. F., & Landstreet, J. D. 1981, ApJS, 45, 457
Beuermann, K. 1988, in Polarized Radiation of Circumstellar Origin, ed. G. V. Coyne, A. F. J. Moffat, S. Tapia, A. M. Magalhaes, R. E. Schulte-Ladbeck, & D. T. Wickramasinghe (Vatican: Vatican Observatory), 125
Cowling, T. G. 1965, in Stars and Stellar Systems, Vol. 8, ed. L. H. Aller & D. B. McLaughlin (Chicago: Univ. Chicago Press), 425
Fontaine, G., & Wesemael, F. 1987, in IAU Colloq. 95, The Second Conference on Faint Blue Stars, ed. A. G. D. Philip, D. S. Hayes, & J. Liebert (New York: Davis), 319
Greenstein, J. L., & Boksenberg, A. 1978, MNRAS, 185, 823
Greenstein, J. L., & Oke, J. B. 1982, ApJ, 252, 285
Jordan, S. 1988, Ph.D. thesis, Institut für Theoretische Physik und Sternwarte der Universitat Kiel
Kemic, S. B. 1974, JILA Rep. 113

Koester, D. 1987, in IAU Colloq. 95, The Second Conference on Faint Blue Stars, ed. A. G. D. Philips, D. S. Hayes, & J. Liebert (New York: Davis), 329
Kurucz, R. 1971, Smithsonian Astrophys. Obs. Spec. Rep. 309
Lamb, D. Q., & Melia, F. 1988, in Polarized Radiation of Circumstellar Origin, ed. G. V. Coyne, A. F. J. Moffat, S. Tapia, A. M. Magalhaes, R. E. Schulte-Ladbeck, & D. T. Wickramasinghe (Vatican: Vatican Observatory), 45
Lamb, F. K., & Sutherland, P. G. 1974, in Physics of Dense Matter, ed. C. J. Hansen (Dordrecht: Reidel), 265
Landstreet, J. D. 1987, MNRAS, 225, 437
Liebert, J., Angel, J. R. P., Stockman, H. S., Spinrad, H., & Beaver, E. A. 1977, ApJ, 214, 457 (L77)
Liebert, J., Fontaine, G., & Wesemael, F. 1987, Mem. Soc. Astron. Ital., 58, 17
Martin, B., & Wickramasinghe, D. T. 1979, MNRAS, 188, 165
———. 1981, MNRAS, 196, 23
Martin, B., & Wickramasinghe, D. T.1982, MNRAS, 200, 993
———. 1984, MNRAS, 206, 407
———. 1986, ApJ, 301, 177 (MW)
Massey, P., Strobel, K., Barnes, J. V., & Anderson, E. 1988, ApJ, 328, 315
Oke, J. B. 1974, ApJS, 27, 21
Schmidt, G. D. 1987, in IAU Colloq. 95, The Second Conference on Faint Blue Stars, ed. A. G. D. Philip, D. S. Hayes, & J. Liebert (New York: Davis), 377
Schmidt, G. D., Weymann, R. J., & Foltz, C. B. 1989, PASP, 101, 713
Shipman, H. L., Liebert, J., & Green, R. F. 1987, ApJ, 315, 239
Sion, E. M., Aannestad, P. A., & Kenyon, S. J. 1988, ApJ, 330, L55
Wendell, C. E., Van Horn, H. M., & Sargent, D. 1987, ApJ, 313, 284
Wickramasinghe, D. T. 1972, MNRAS, 76, 129
———. 1987, in IAU Colloq. 95, The Second Conference on Faint Blue Stars, ed. A. G. D. Philip, D. S. Hayes, & J. Liebert (New York: Davis), 389